

A novel dual-channel thermo-optic locking method for the whisperinggallery mode microresonator

Wenjie Fan(范文杰), Wenyao Liu(刘文耀), ZiwenPan(潘梓文), Rong Wang(王蓉), Lai Liu(刘来), EnboXing(邢恩博), Yanru Zhou(周彦汝), Jun Tang(唐军), and Jun Liu(刘俊)

Citation: Chin. Phys. B, 2024, 33 (**5**): 054206. DOI: 10.1088/1674-1056/ad225f
Journal homepage: http://cpb.iphy.ac.cn; http://iopscience.iop.org/cpb

What follows is a list of articles you may be interested in

Improving resolution of superlens based on solid immersion mechanism

Zhanlei Hao(郝占磊), Yangyang Zhou(周杨阳), Bei Wu(吴贝),Yineng Liu(刘益能), and Huanyang Chen(陈焕阳)
Chin. Phys. B, 2023, 32 (**6**): 064211. DOI: 10.1088/1674-1056/ac8726

Mode characteristics of VCSELs with different shape and size oxidation apertures

Xin-Yu Xie(谢新宇), Jian Li(李健), Xiao-Lang Qiu(邱小浪), Yong-Li Wang(王永丽), Chuan-Chuan Li(李川川), and Xin Wei(韦欣)
Chin. Phys. B, 2023, 32 (**4**): 044206. DOI: 10.1088/1674-1056/ac9821

Optomagnonically tunable whispering gallery cavity laser wavelength conversion

Yining Zhu(朱奕宁), Zixu Zhu(朱子虚), Anbang Pei(裴安邦), and Yong-Pan Gao(高永潘)
Chin. Phys. B, 2023, 32 (**2**): 024206. DOI: 10.1088/1674-1056/ac7862

Single-mode lasing in a coupled twin circular-side-octagon microcavity

Ke Yang(杨珂), Yue-De Yang(杨跃德), Jin-Long Xiao(肖金龙), and Yong-Zhen Huang(黄永箴)
Chin. Phys. B, 2022, 31 (**9**): 094205. DOI: 10.1088/1674-1056/ac6802

Resonantly driven exciton Rabi oscillation in single quantum dots emitting at 1300 nm

Yong-Zhou Xue(薛永洲), Ze-Sheng Chen(陈泽升), Hai-Qiao Ni(倪海桥), Zhi-Chuan Niu(牛智川), De-Sheng Jiang(江德生), Xiu-Ming Dou(窦秀明), Bao-Quan Sun(孙宝权)
Chin. Phys. B, 2017, 26 (**8**): 084202. DOI: 10.1088/1674-1056/26/8/084202

A novel dual-channel thermo-optic locking method for the whispering gallery mode microresonator

Wenjie Fan(范文杰)[1], Wenyao Liu(刘文耀)[1,2,†], Ziwen Pan(潘梓文)[1], Rong Wang(王蓉)[1], Lai Liu(刘来)[1,2], Enbo Xing(邢恩博)[1,2], Yanru Zhou(周彦汝)[1,2], Jun Tang(唐军)[1,2], and Jun Liu(刘俊)[1,2]

[1] *State Key Laboratory of Dynamic Measurement Technology, North University of China, Taiyuan* 030051, *China*
[2] *Shanxi Province Key Laboratory of Quantum Sensing and Precision Measurement, North University of China, Taiyuan* 030051, *China*

(Received 5 December 2023; revised manuscript received 8 January 2024; accepted manuscript online 25 January 2024)

Mode locking can be effectively achieved by using the thermo-optic effects in the whispering gallery mode (WGM) optical microcavity, without the help of external equipment. Therefore, it has the advantages of small size, low integration costs, and self-locking, which shows great potential for application. However, the conventional single-channel microcavity thermal-locking method that relies solely on internal thermal balance will inevitably be disturbed by the external environment. This limitation affects the locking time and stability. Therefore, in this paper, we propose a new method for closed-loop thermal locking of a dual-channel microcavity. The thermal locking of the signal laser and the thermal regulation of the control laser are carried out respectively by synchronously drawing a dual-path tapered fiber. The theoretical model of the thermal dynamics of the dual-channel microcavity system is established, and the influence of the control-laser power on the thermal locking of the signal laser is confirmed. The deviation between the locking voltage of the signal laser and the set point value is used as a closed-loop feedback parameter to achieve long-term and highly stable mode locking of the signal laser. The results show that in the 2.63 h thermal-locking test, the locking stability is an order of magnitude higher than that of the single tapered fiber. This solution addresses the issue of thermal locking being disrupted by the external environment, and offers new possibilities for important applications such as spectroscopy and micro-optical sensor devices.

Keywords: optical microcavity, thermo-optic locking, thermal nonlinearity effect

PACS: 42.55.Sa, 78.20.N–, 42.65.Sf, 42.60.Da **DOI:** 10.1088/1674-1056/ad225f

1. Introduction

Whispering gallery mode (WGM) optical microcavities[1] have the characteristics of a high quality factor (Q) and a small mode volume, which can greatly enhance the interaction between light and matter. They are widely used in high-sensitivity sensing,[2–4] nonlinear optics,[5–8] microlasers,[9–11] cavity optomechanics,[12–15] and quantum information.[16] Noteworthy in these applications is the precise wavelength matching between the signal laser and the microcavity resonance, necessitating a stable level of detuning between them. Methods to solve this problem include actively locking the signal-laser wavelength to the microcavity resonance (e.g., Pound–Drever–Hall technology[17]) or tuning the resonance of the resonator itself to match the signal-laser wavelength (commonly used microcavity thermal-locking technology[18]). PDH locking technology is widely used due to its high-precision frequency locking. Compared with PDH locking technology, micro-cavity thermal locking does not need to add other equipment, and has the advantages of simple structure, good flexibility and convenient operation. When the signal-laser wavelength is located in the blue detuning region of the microcavity resonance, the mode thermal locking can be realized using the broadened resonance peak in the bistable effects. This active locking method has good stability and great potential in high-precision sensing and information-detection applications.

Carmon *et al.* were the first to focus on thermal effects within microcavities, establishing a thermodynamic model for microcavities and explaining the bistable behavior observed in microcavities over timescales. They demonstrated the existence of a stable state within the broadened resonance peak in the blue detuned region, both theoretically and experimentally. This state effectively maintained the signal-laser wavelength within the resonance peak, achieving mode locking. However, this method was susceptible to environmental disturbances, which hindered long-term stability.[18] Subsequently, Carmon *et al.* proposed a locking method using signal-laser power as a feedback control parameter, thereby reducing the number of components compared to PDH locking techniques. This method achieves self-stabilization through thermal equilibrium and introduces closed-loop feedback. However, the strength of the feedback was determined by the power of the signal laser, which limited the stability of thermal locking.[19] Li *et al.* conducted a theoretical analysis of frequency fluctuations in microcavities under thermal-optic locking conditions and experimentally measured the corresponding frequency fluctuation spectrum. They found that locking relative frequency fluctuations led to temperature fluctuations within

[†]Corresponding author. E-mail: liuwenyao@nuc.edu.cn

© 2024 Chinese Physical Society and IOP Publishing Ltd

the microcavity, transferring frequency noise onto the cavity's locking mode. However, this did not improve thermal-locking time or stability.[20] Zhang *et al.* established a thermodynamic model using simulation and experimentation, by considering parameters such as microcavity size, scanning speed, and the impact of laser power on microcavity structure. They developed a locking device that is induced by thermal effects, by adjusting internal parameters to increase the locking time to 1.1 h. However, the device remained susceptible to external environmental interference.[21] Similarly, Agarwal *et al.* utilized a broadened resonance peak to lock the resonator in a specific mode. Under high-power signal lasers, the resonator self-tunes to a fixed wavelength despite environmental temperature changes. However, under low-power lasers, the resonator was prone to losing lock.[22] The challenge of achieving long-term and highly stable thermal locking, impervious to environmental disturbances, without adding additional equipment, remains a significant hurdle.

In this paper, we propose a novel approach, the dual-channel microcavity closed-loop thermal-locking system. We extended the classical single-path microcavity thermal dynamic model by introducing the influence of control-laser power on the thermal-locking mode of the signal laser. By leveraging the thermo-optic effects of the control laser on the microcavity, we have enhanced the locking time and stability of the signal laser. Additionally, we have innovatively introduced a synchronized dual-path tapered optical fiber fabrication process, which allows precise control of the diameters of the dual tapered regions and the spacing between them. This enables simultaneous coupling with a single microsphere cavity, enabling both paths to concurrently excite high optical Q-factor whispering gallery modes (WGM). This method separates the thermal locking of the signal laser from the thermal modulation of the control laser, providing a new approach to improve the duration and stability of thermal locking.

2. Theoretical model

Based on the classical resonant cavity thermal tuning theory, an extension is made to the single-channel microresonator thermal dynamics model by introducing an additional control laser. Both the signal and control lasers utilize a thermal-locking method to fix their respective wavelengths. By adjusting the power of the control laser, the temperature of the microresonator changes, which in turn regulates the thermal locking of the signal laser. Ultimately, this establishes a dual-channel microresonator thermal-locking system. The resonant wavelength depends on the refractive index (n) and the diameter (D) of the microsphere cavity. The change in the resonant wavelength of a silica microsphere due to temperature can be expressed as follows:[23]

$$\Delta\lambda(\Delta T) = \lambda_0\left(\frac{1}{n}\frac{\mathrm{d}n}{\mathrm{d}T}\Delta T + \frac{1}{D}\frac{\mathrm{d}D}{\mathrm{d}T}\Delta T\right) = \lambda_0\alpha\Delta T, \quad (1)$$

where λ_0 is the resonant wavelength of the cold microsphere cavity. Here, $\mathrm{d}n/\mathrm{d}T$ and $\mathrm{d}D/\mathrm{d}T$ are the thermo-optic coefficient and thermal expansion coefficient of the microsphere cavity. We define α as the temperature coefficient for silica material, which includes both thermal expansion and thermo-optic effects. For wavelengths near $\lambda_0 = 1550$ nm, the temperature coefficient $\alpha = 6\times10^{-6}$ K^{-1} for silica.[24] Consequently, we can express the resonant wavelength λ_r as a function of temperature using the following equation:

$$\lambda_\mathrm{r}(\Delta T) = \lambda_0 + \Delta\lambda(\Delta T) = \lambda_0(1+\alpha\Delta T). \quad (2)$$

The heat introduced into the microsphere cavity by the laser consists of four components: (i) laser power (I), (ii) optical coupling efficiency (η), (iii) the effect of laser absorption on the resonant cavity, and (iv) the deviation between the laser wavelength (λ_l) and the microsphere cavity's resonant wavelength (λ_r). Thus, the thermal energy entering the cavity due to the laser is described by the following equation:[18]

$$\begin{aligned}\dot{q}_\mathrm{in} &= I\eta\frac{Q}{Q_\mathrm{abs}}\frac{1}{\left(\dfrac{\lambda_\mathrm{l}-\lambda_\mathrm{r}}{\delta\lambda/2}\right)^2+1}\\ &= I_\mathrm{h}\frac{1}{\left(\dfrac{\lambda_\mathrm{l}-\lambda_0(1+\alpha\Delta T)}{\delta\lambda/2}\right)^2+1},\end{aligned} \quad (3)$$

where $\delta\lambda$ is the resonance bandwidth, Q is the optical quality factor of the microsphere cavity, and Q_abs is the quality factor resulting from absorption losses within the microsphere cavity. To simplify the equation and facilitate the discussion on specific parameters influencing the temperature of the cavity, we define the power heating the cavity by the laser as $I_\mathrm{h} = I\eta Q/Q_\mathrm{abs}$. Additionally, we utilize the temperature-dependent expression for the resonant wavelength λ_r, as described in Eq. (2).

Based on the law of conservation of energy, the temperature change ΔT in the microsphere cavity caused by the laser is determined by the difference between the incoming heat (q_in) and the outgoing heat (q_out)

$$\begin{aligned}C_\mathrm{p}\Delta\dot{T}(t) &= \dot{q}_\mathrm{in} - \dot{q}_\mathrm{out}\\ &= I_\mathrm{h}\frac{1}{\left(\dfrac{\lambda_\mathrm{l}-\lambda_0(1+\alpha\Delta T)}{\delta\lambda/2}\right)^2+1} - K\Delta T(t),\end{aligned} \quad (4)$$

where C_p is the equivalent heat capacity (J·K^{-1}) of the mode volume, and K is the equivalent thermal conductivity (W·m^{-1}·K^{-1}) between the optical mode volume and the rest of the spherical cavity.

According to Eq. (4), we obtained the laser transmission spectrum influenced by the opto-thermal effects. As the laser

shifts towards longer wavelengths, the resonance peak broadens. Conversely, as the laser moves towards shorter wavelengths, the resonance peak compresses, resulting in a thermal bistable phenomenon, as illustrated in Fig. 1(a). Subsequently, by adjusting the laser's scanning speed and range, mode locking can be achieved within a single scanning cycle, building upon the bistable effect, as shown in Fig. 1(b). Following thermal locking, alterations in the external environmental temperature can affect the thermal-locking performance of the microcavity, particularly impacting the locking time and stability. The dual-channel microcavity closed-loop thermal-locking system couples an additional control laser with the conventional single-path signal laser. Both the signal laser and control laser utilize the thermal-locking method to stabilize their wavelengths around the resonant wavelength. By modulating the power of the control laser, changes in the microsphere's temperature are induced, thereby regulating and optimizing the thermal locking of the signal laser.

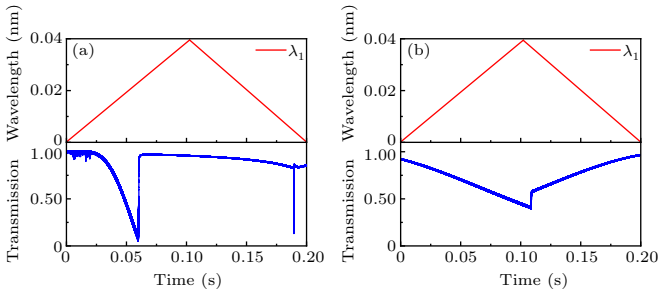


Fig. 1. (a) The bistable response curve (blue) during laser wavelength scanning (red). (b) Achieving mode locking (blue) throughout the entire scanning cycle (red) using thermal nonlinearity effects.

Thus, we have derived the thermodynamic equations for the dual-channel microcavity closed-loop thermal-locking system associated with the control-laser power I_{hc}:

$$\begin{cases} C_{\mathrm{ps}}\Delta\dot{T}_{\mathrm{s}}(t) = I_{\mathrm{hs}}\dfrac{1}{\left(\dfrac{\lambda_{\mathrm{s}}-\lambda_{\mathrm{r}}}{\delta\lambda/2}\right)^2+1} - K_{\mathrm{s}}\Delta T_{\mathrm{s}}(t), \\ C_{\mathrm{pc}}\Delta\dot{T}_{\mathrm{c}}(t) = I_{\mathrm{hc}}\dfrac{1}{\left(\dfrac{\lambda_{\mathrm{c}}-\lambda_{\mathrm{r}}}{\delta\lambda/2}\right)^2+1} - K_{\mathrm{c}}\Delta T_{\mathrm{c}}(t), \\ \lambda_{\mathrm{r}}(\Delta T_{\mathrm{c}}) = \lambda_0(1+\alpha\Delta T_{\mathrm{c}}), \end{cases} \tag{5}$$

where C_{ps} and C_{pc} are the equivalent heat capacities of the signal laser and control laser's respective mode volumes. Here, ΔT_{s} and ΔT_{c} are the temperature changes induced by the signal laser and control laser in the microcavity; λ_{s} and λ_{c} are the wavelengths of the signal laser and control laser, respectively; I_{hs} and I_{hc} are the powers of the signal laser and control laser. Currently, the system is in a locked state, where λ_{s} and λ_{c} are fixed. We can change the control-laser power (I_{hc}) to adjust the microsphere cavity temperature (ΔT_{c}), and consequently alter the resonance wavelength (λ_{r}) of the microsphere cavity. Ultimately, this achieves modulation of the thermal locking of the signal laser by the control laser.

Based on the aforementioned theoretical model, the relationship between the maximum equivalent temperature change (ΔT) of the microcavity and the power of the control laser can be determined, as shown in Fig. 2. When the laser power is less than 1 mW, the maximum temperature change in the microcavity is approximately 0.11 K, while at 10 mW, the maximum temperature change in the microcavity is about 11 K. Therefore, when the signal-laser power is set to 1 mW and the control-laser power is set to 10 mW, the temperature change in the microcavity caused by the signal laser is only one percent of that caused by the control laser. At this point, the temperature change in the microcavity caused by the signal laser can be considered negligible while adjusting the thermal locking of the signal laser by modifying the power of the control laser. Additionally, when the power exceeds 7 mW, there is a linear correlation between the microcavity's temperature variation and the power. The resonant position of the signal laser's thermal-locking mode follows a linear variation, as described by Eq. (5). This provides theoretical guidance for selecting the power levels of both the signal and control lasers in experimental setups.

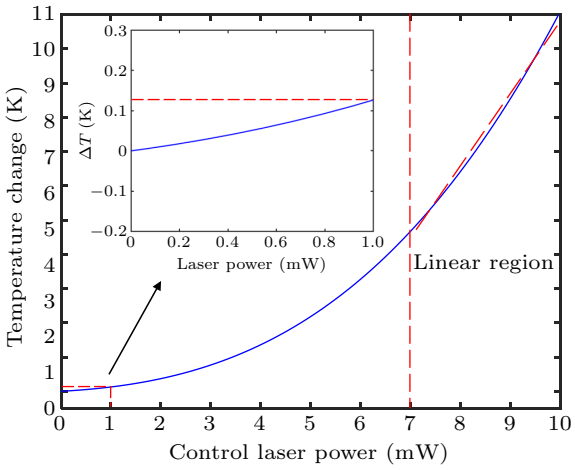


Fig. 2. The relationship between the maximum equivalent temperature change in the microcavity and the control-laser power. The inset indicates that when the laser power is less than 1 mW, the maximum temperature change in the microsphere cavity is approximately 0.11 K. The parameters used for the fit are $\eta = 0.8$, $\lambda_0 = 1548.23$ nm, $Q = 4\times10^7$, $Q_{\mathrm{abs}} = 2\times10^{10}$, and $\Delta\lambda = -0.065$ nm.

3. Device fabrication and experimental setup

The traditional tapered-fiber coupling system involves injecting the signal laser into the microsphere through one tapered fiber. We augmented this setup by introducing another tapered fiber to couple the control laser, thereby creating a dual-channel microcavity coupling system, as depicted in Fig. 3(a). To achieve optimal coupling with the microsphere, it is essential to ensure that the diameters of two ta-

pered fibers are approximately equal. Additionally, if the separation between the tapers is too large (exceeding the diameter of the microsphere cavity), simultaneous coupling with the microsphere becomes impossible. Conversely, if the separation is too small, it might lead to mutual interference between the optical modes of the two lasers. Consequently, achieving simultaneous excitation of high optical Q-factor WGMs in a dual-channel microcavity system poses challenges, necessitating precise control over the diameters and separation of the two tapered regions.

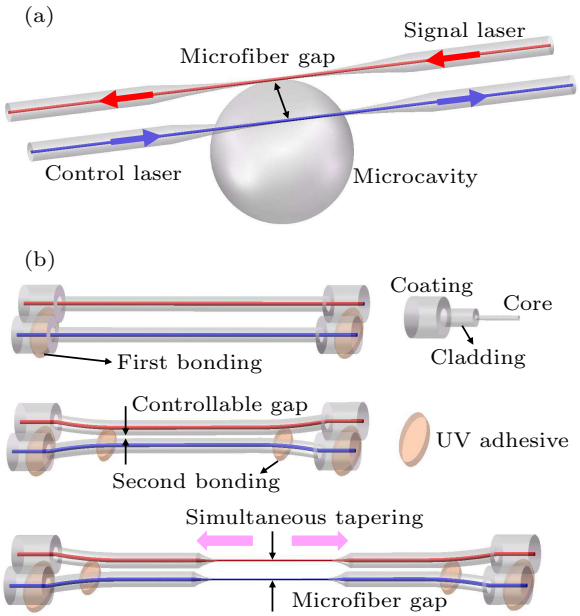


Fig. 3. (a) A dual-path tapered optical fiber coupled with a microsphere cavity. (b) The fabrication method of the dual-path tapered optical fibers.

To address this, we propose a fabrication process for dual-path tapered optical fibers, as illustrated in Fig. 3(b). Initially, the coating layer is removed from two single-mode optical fibers (core/cladding 9/125 μm). UV adhesive is then used to bond the coating at both ends of the cladding in parallel, shaping them preliminarily. Subsequently, a second bonding procedure is performed at the edges of the cladding, during which opposing forces are applied to precisely control the distance between the cladding layers of the two optical fibers. Finally, by employing a hydrogen–oxygen flame, both optical fibers are simultaneously heated, resulting in a one-time drawing of tapered regions with diameters of 1 μm–3 μm and a pitch of 70 μm–90 μm. Real-time monitoring of the spacing and transmission of the dual-path tapered optical fibers is conducted throughout the entire preparation process using a CCD and a host computer to ensure precise control over their diameters and modes. Additionally, to fabricate quartz microsphere resonators with a high optical Q-factor and match them with the dual-path tapered fibers, we utilized a CO_2 laser to melt quartz single-mode fibers at high temperatures. Control over the diameters and sphere-to-stem ratios of the microspheres could be easily managed by regulating the laser power and focal length.

The experimental setup is illustrated in Fig. 4. A tunable laser (TOPTICA CTL-1550) with a linewidth of 10 kHz serves as the pump laser. The wavelength is linearly scanned using a triangular waveform generated by a function signal generator (GWINSTEK AFG-2225). The output laser is amplified through an isolator and an erbium-doped fiber amplifier (Thorlabs EDFA100S). It is then split into two paths using a 1×2 splitter (Thorlabs PFC 1550 F) to create the signal laser and the control laser. Both laser paths are connected to an acousto-optic modulator (G-1550-40-L-B-T-AA-A-T-L) and an attenuator (VOA50PM-APC) to fine-tune the wavelength and power. These paths are coupled into a microsphere cavity via dual-path tapered optical fibers, where the coupling position is monitored by a CCD camera (SANQTD TD-508 A), and the output power is measured by an optical power meter with a probe (Thorlabs S155 C). Two independent polarization controllers are used to adjust the polarization and achieve optimal coupling strength. The output optical signals from the two paths are detected by two photodetectors (PD Thorlabs DET 08 CFC) and monitored using an oscilloscope (Tektronix MSO 64) to observe the transmission spectrum of both paths. We use the deviation between the locked voltage of the signal laser and its setpoint as feedback parameters, inputting them into AOM-1 in the control path. The PID automatic feedback adjusts the input current of AOM-1, regulating the power of the control laser in real time.

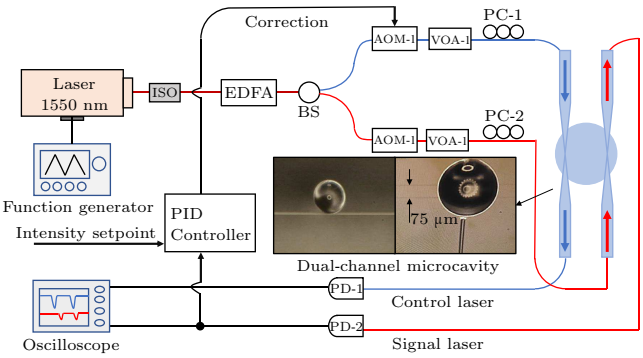


Fig. 4. A schematic of the experimental setup. ISO: isolator, PC: polarization controller, EDFA: erbium-doped fiber amplifier, AOM: acousto-optic modulator, CCD: CCD camera, BS: beam splitter, VOA: variable optical attenuator, PD: photodetector, PID: proportional-integral-derivative. The inset comprises a top view and a side view of the coupling between dual-path tapered optical fibers and a microsphere cavity under electron microscopy. The microsphere diameter is 300 μm, and the separation between the dual tapered regions is 75 μm.

4. Results and discussion

In the experiment, we set the output power of the signal laser to 1 mW and the output power of the control laser to 10 mW. We first set the laser's rapid wavelength scanning parameters. The scanning voltage of the laser is 10 V, and the scanning frequency is 10 Hz. By using an oscilloscope, we can

observe the optical modes of the two lasers in real time and obtain the transmission spectra of the signal laser and the control laser. The transmission spectra of the two lasers are different, as shown in Fig. 5(a), indicating that the optical modes are isolated. Figures 5(c) and 5(e) are local enlargements of Fig. 5(a). We adjusted the scanning range of the laser and selected the resonant wavelength with a higher optical Q factor, reducing the scanning frequency of the laser. The scanning voltage of the laser is 10 V, and the scanning frequency is 1 Hz. During this scanning cycle, the accumulation of thermal effects achieves mode locking of the signal laser and the control laser, as shown in Fig. 5(b). Finally, the laser stopped scanning, and the signal laser and control laser were individually locked near the microsphere cavity resonance wavelength, as shown in Figs. 5(d) and 5(f). The yellow point in Fig. 5(c) represents the locking position of the control laser in the spectrum, while the green point in Fig. 5(d) represents the locking position of the signal laser in the spectrum. In the experiment, the microsphere cavity radius was 150 μm, the Q factor of the control optical path was 4.17×10^7, and the Q factor of the signal optical path was 2.79×10^7.

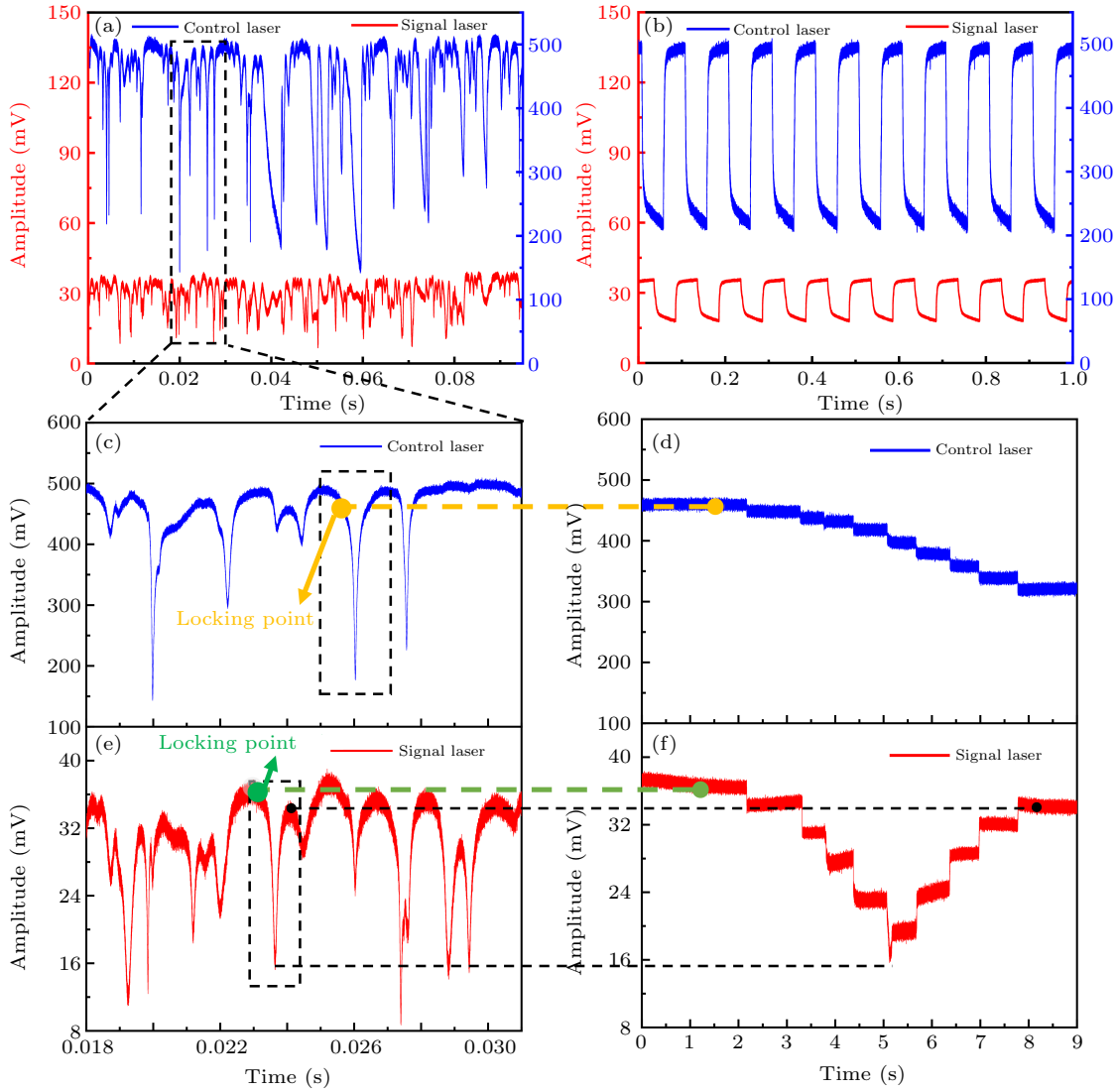


Fig. 5. (a) The transmission spectrum of the signal laser and the control laser demonstrates the isolation of their optical modes. (b) Achieved mode-locking of the signal laser and the control laser throughout the scanning cycle using thermal nonlinearity effects. The scanning voltage of the laser is 10 V, and the scanning frequency is 1 Hz. (c) A close-up of the transmission spectrum during the rapid scanning of the control laser in (a), with the yellow dot indicating the locked position of the control laser in the spectrum. (d) The laser stopped scanning. The decrease in the power of the control laser, resulting in a decrease in voltage amplitude. (e) A close-up of the transmission spectrum during the rapid scanning of the signal laser in (a), with the green dot indicating the locked position of the signal laser in the spectrum. (f) The laser stopped scanning. The decrease in the control-laser power results in a shift in the thermal-locking position of the signal laser. This shift reflected a complete transmission spectrum, which corresponds to one transmission spectrum during rapid scanning of the signal laser.

At this time, both the signal laser and the control laser are locked. We systematically decrease the power of the control laser in a linear manner to reduce the number of photons absorbed by the microsphere cavity. Consequently, the temperature of the microcavity decreases linearly, as described by Eq. (5), resulting in a linear decrease in the resonance

wavelength of the microcavity, and causing a blue shift in the resonance wavelength. In this phase, the wavelength of the signal laser remains fixed while the resonance wavelength of the microsphere cavity undergoes a blue shift, equivalent to a red shift of the signal-laser wavelength within the blue detuning region. This process effectively reconstructs the complete transmission spectrum of the signal laser, as illustrated in Fig. 5(f). It corresponds to one of the transmission spectra during rapid scanning, as depicted in Fig. 5(e). The alterations in the signal laser's transmission due to variations in the microcavity's resonance wavelength correspond well to the transmission spectrum observed during rapid scanning. Their resonance depths exhibit consistency. In this experiment, the tuning range of the control laser in the signal laser's thermal-locking mode is 2.85×10^9 Hz, with a tuning sensitivity of 1.58×10^7 Hz/mW.

We also measured the response time of the thermal-locking mode of the signal laser modulated by the control laser, as shown in Fig. 6. At this time, both the signal laser and the control laser are locked. The control laser was modulated using a $LiNbO_3$ intensity modulator (LN81S-FC) with a square wave voltage at 2 Hz. The measured rise time was 4.8 milliseconds, and the fall time was 3.96 milliseconds. By employing microspheres with smaller dimensions, the thermal conduction time within the microsphere cavity can be accelerated, leading to further improvement in response speed.

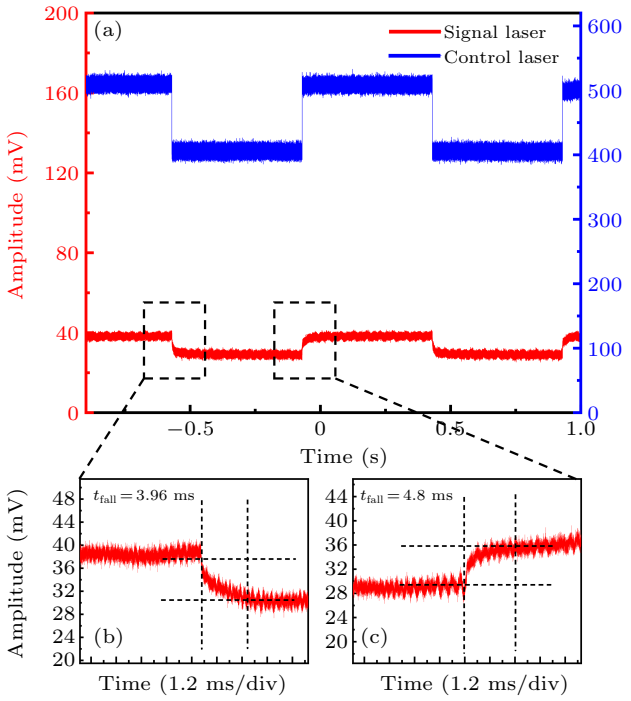


Fig. 6. The response time of the signal laser's thermal-locking position variation caused by changes in the power of the control laser. (a) The thermal-locking position variation diagram for the control laser and the signal laser. (b) The falling edge. (c) The rising edge.

We use the deviation between the locked voltage of the signal laser and its setpoint as feedback parameters, inputting them into AOM-1 in the control path. The PID automatic feedback adjusts the input current of AOM-1, regulating the power of the control laser in real time, thereby aligning the signal laser to its resonance nadir. In the experiment, the power of the signal laser in the dual-channel microresonator coupled system was set to 1 mW, while the power of the control laser was set to 0 mW and 10 mW, corresponding to Figs. 7(a) and 7(b), respectively. The results indicate that, under the same coupling conditions and external environment, the addition of closed-loop feedback (with the control laser power set at 10 mW) increased the locking duration of the signal laser from 0.44 h to 2.63 h, compared to the traditional single-channel thermal locking of the signal laser (with the control-laser power set at 0 mW). Furthermore, the maximum voltage amplitude variation decreases from 6 mV to 0.5 mV, demonstrating a twelve-fold increase in stability.

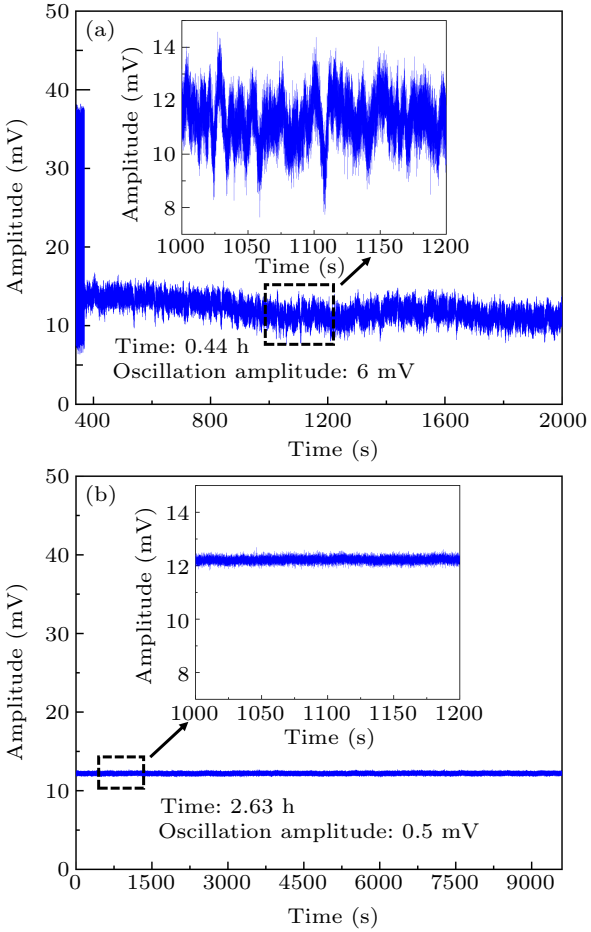


Fig. 7. (a) Traditional single-channel thermal locking of the signal laser. (b) Thermal locking of the signal laser in a dual-channel microcavity with closed-loop feedback.

5. Conclusion and perspectives

In summary, microcavity thermal locking offers advantages such as a simple structures and convenient operation. It has found widespread application in establishing stable frequency detuning between external lasers and microcavities.

However, the thermal equilibrium of thermal locking is susceptible to external environmental disturbances, which limits its locking time and stability. In this paper, we propose a novel dual-channel microcavity closed-loop thermal-locking method. By employing synchronized dual-path tapered optical fibers, the thermal locking of the signal laser and the thermal modulation of the control laser are separated. We establish a thermodynamic theoretical model for the dual-channel microcavity system and verify the influence of the control-laser power on the thermal locking of the signal laser. The tuning range of the control laser in the thermal-locking mode of the signal laser is 2.85×10^9 Hz, with a tuning sensitivity of 1.58×10^7 Hz/mW. Using the deviation between the voltage of the signal laser's locking point and the setpoint as feedback parameters, PID automatic feedback adjustment controls the power of the control laser, achieving long-term and highly stable mode locking of the signal laser. The results indicate that compared to thermal locking with a single-path tapered optical fiber, the locking time of the signal laser has increased from 0.44 h to 2.63 h, improving stability by an order of magnitude. Importantly, this method does not require adjustment of the power of the signal laser, making it applicable across various signal-laser power levels. This new approach addresses the issue of thermal locking, which is susceptible to environmental interferences, providing a new avenue for laser tuning, and has significant potential for high-precision sensing and information-detection applications.

Acknowledgments

Project supported by the National Key Research and Development Program of China (Grant No. 2022YFB3203400), the National Natural Science Foundation of China (Grant Nos. U21A20141, 62273314, and 51821003), the Fundamental Research Program of Shanxi Province (Grant No. 202303021223001), and Shanxi Province Key Laboratory of Quantum Sensing and Precision Measurement (Grant No. 201905D121001).

References

[1] Vahala K J 2003 *Nature* **424** 839
[2] Foreman M R, Swaim J D and Vollmer F 2015 *Adv. Opt. Photon.* **7** 168
[3] Toropov N, Cabello G, Serrano M P, Gutha R R, Rafti M and Vollmer F 2021 *Light: Science & Applications* **10** 42
[4] Chen C and Wang J 2020 *Analyst* **145** 1605
[5] Gaeta A L, Lipson M and Kippenberg T J 2019 *Nat. Photon.* **13** 158
[6] Spencer D T, Drake T, Briles T C, Stone J, Sinclair L C, Fredrick C, Li Q, Westly D, Ilic B R and Bluestone A 2018 *Nature* **557** 81
[7] Kasumie S, Lei F, Ward J M, Jiang X, Yang L and Nic Chormaic S 2019 *Laser Photonics Rev.* **13** 1900138
[8] Lin G, Coillet A and Chembo Y K 2017 *Adv. Opt. Photonics* **9** 828
[9] Yang L, Armani D and Vahala K 2003 *Appl. Phys. Lett.* **83** 825
[10] Jiang X F, Zou C L, Wang L, Gong Q and Xiao Y F 2016 *Laser Photonics Rev.* **10** 40
[11] He L, Özdemir Ş K and Yang L 2013 *Laser Photonics Rev.* **7** 60
[12] Aspelmeyer M, Kippenberg T J and Marquardt F 2014 *Rev. Mod. Phys.* **86** 1391
[13] Jiang X, Wang M, Kuzyk M C, Oo T, Long G L and Wang H 2015 *Opt. Express* **23** 27260
[14] Monifi F, Zhang J, Özdemir Ş K, Peng B, Liu Y X, Bo F, Nori F and Yang L 2016 *Nat. Photon.* **10** 399
[15] Dong C, Fiore V, Kuzyk M C and Wang H 2012 *Science* **338** 1609
[16] Khalili F Y and Danilishin S L 2016 *Prog. Opt.* **61** 113
[17] Black E D 2001 *Am. J. Phys.* **69** 79
[18] Carmon T, Yang L and Vahala K J 2004 *Opt. Express* **12** 4742
[19] Carmon T, Kippenberg T J, Yang L, Rokhsari H, Spillane S and Vahala K J 2005 *Opt. Express* **13** 3558
[20] Li J, Diddams S and Vahala K J 2014 *Opt. Express* **22** 14559
[21] Zhang B, Liu W, Wang R, Pan Z, Li W, Wang X, Zhou Y, Xing E, Tang J and Liu J 2023 *Opt. Commun.* **530** 129150
[22] Agarwal M and Teraoka I 2012 *Appl. Phys. Lett.* **101** 251105
[23] Dong C H, He L, Xiao Y F, Gaddam V, Ozdemir S, Han Z F, Guo G C and Yang L 2009 *Appl. Phys. Lett.* **94** 231119
[24] Leviton D B and Frey B J 2006 *Optomechanical Technologies for Astronomy* **6273** 800